crystals

MDPI

Article

Synthesis and Spectroscopic Characterizations of Some Essential Metal Ion (Mg^{II}, Ca^{II}, Zn^{II}, and Fe^{III}) Pipemidic Acid Chemotherapeutic Agent Complexes

Asma S. Al-Wasidi

Department of Chemistry, College of Science, Princess Nourah Bint Abdulrahman University, Riyadh 11671, Saudi Arabia; asalwasidi@pnu.edu.sa

Abstract: The assignments structures of the four 1:1 pipemidic acid (pipH)–magnesium(II), calcium(II), zinc(II), and iron(III) complexes, $[Mg(pip)(H_2O)_3(Cl)].6H_2O$, $[Ca(pip)(H_2O)_3(Cl)].2H_2O$, $[Zn(pip)(H_2O)_3(Cl)].4H_2O$, and $[Fe(pip)(H_2O)_2(Cl)_2].6H_2O$, (where pip = deprotonated pipemidic), were synthesized through the chemical reactions of $MgCl_2.6H_2O$, $CaCl_2.2H_2O$, $ZnCl_2$, and $FeCl_3.6H_2O$ metal salt chlorides with pipH chemotherapeutic agent ligand in a methanolic solvent. The microanalytical analysis CHN, conductance, (infrared (FTIR) and electronic (UV–Vis.)) spectra, and thermogravimetric measurements (TG) have been utilized to discuss the solid isolated complexes. The X-ray powder diffraction (XRD) analysis and the transmission electron microscopy (TEM) confirm the nanostructured form of the synthesized pip complexes. The deprotonated pipH ligand is coordinated to Mg(II), Ca(II), Zn(II), and Fe(III) metal ions through the two oxygen atoms of the carbonyl (quinolone group) and carboxylic group. The thermodynamic parameters (energy, E*), (entropy, ΔS*), (enthalpy, ΔH*), and (Gibbs free energy, ΔG*) of activation have been estimated based on thermogravimetric curves using "Coats–Redfern and Horowitz–Metzeger non–isothermal" methods.

Keywords: pipemidic acid; complexes; FTIR; XRD; TEM

check for updates

Citation: Al-Wasidi, A.S. Synthesis and Spectroscopic Characterizations of Some Essential Metal Ion (Mg^{II}, Ca^{II}, Zn^{II}, and Fe^{III}) Pipemidic Acid Chemotherapeutic Agent Complexes. *Crystals* **2023**, *13*, 596. https://doi.org/10.3390/cryst13040596

Academic Editor: Marian Valko

Received: 8 March 2023
Revised: 20 March 2023
Accepted: 30 March 2023
Published: 1 April 2023

Copyright: © 2023 by the author. Licensee MDPI, Basel, Switzerland. This article is an open access article distributed under the terms and conditions of the Creative Commons Attribution (CC BY) license (https://creativecommons.org/licenses/by/4.0/).

1. Introduction

A pyridopyrimidine chemotherapeutic agent derivative of piperidic acid, pipemidic acid (pipH, Figure 1), has an action against both Gram-negative and certain Gram-positive bacteria. In comparison to pyromedic acid and nalidixic acid, pipemidic acid is more active, and it also has a reasonable amount of action against pyromedic acid- and nalidixic acid-resistant bacteria. A pyridopyrimidine, pipemidic acid is a 5-oxo-5,8-dihydropyrido[2,3-d]pyrimidine-6-carboxylic acid that has an ethyl group at position 8 and a piperazine-1-yl group at position 2 replaced. A broad-spectrum chemotherapeutic agent used to treat infections of the biliary, digestive, and urinary tracts. It has a role as an antibacterial drug and an inhibitor of DNA synthesis. It is a monocarboxylic acid, an amino acid, an N-arylpiperazine, a pyridopyrimidine, and a quinolone chemotherapeutic agent.

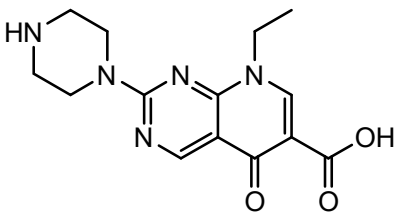


Figure 1. Molecular structure of pipemidic acid (pipH).

It is worth noting that the marketing authorization of pipemidic acid has been suspended throughout the EU due to the adverse side effects [1]. A special focus has been

placed on how metal ions interact with antibiotics when discussing how medications and cations of metals interact in biochemical processes. A family of medications known as the Cross-reaction of antibiotics with cations of metals has been extensively employed in medicine to treat both people and animals [2]. Particularly, the relationship among beta-lactam antibiotics like "cephalexin", and transition metals has been studied using a variety of physical, chemical, and spectroscopic approaches as well as extensive biological data [3–6]. When administered in the form of metal complexes, many medications have altered pharmacokinetic and toxicological characteristics. Copper(II), which has been proven effective against various illnesses, including cancer, rheumatoid arthritis, gastric ulcers, and TB, may be the most thoroughly investigated cation in this area [7–10]. Since nalidixic acid's discovery around 4 decades ago, the number of medications belonging to the quinolone family has increased exponentially. Since then, this family's exponential development has created over 10,000 mimics [11]. The chemistry of these medicines' coordination with biologically and pharmacologically relevant metal ions is quite interesting. The top member of the first-generation quinolone family was thought to be pipemidic acid. Crystal structure determination and production of quinolone derivative-containing metal complexes have been the subject of several investigations [12–15]. Quinolone chemotherapeutic agents have a number of potential roles in complex formation [16–20]. Only the electrostatic interaction between the drug and the metal ions is seen in these complexes in the event of isolation because they often comprise single and/or double-protonated quinolones that can bind to the metal ion [16–18]. However, [19–21] discovered that neutral quinolones may form simple complexes in the zwitterionic state (bidentate chelate). Quinolones are also capable of serving as binding bridges, which allows them to create polynuclear complexes [20,21]. Understanding the drug–metal ion interaction and the possible pharmacological applications of a 1:1 molar ratio metal complex with quinolone chemotherapeutic drug agents is crucial. This work reports the isolation and characterization of the complex magnesium, calcium, zinc, and iron cations. The hypothesized structures of the complexes produced by this reaction were deduced using FTIR spectroscopy, electronic spectra, and thermogravimetric analyses.

2. Experimental

2.1. Chemicals

All chemicals and reagents mentioned in this article ($MgCl_2.6H_2O$, $CaCl_2.2H_2O$, $ZnCl_2$, $FeCl_3.6H_2O$, and pipemidic acid in Figure 1) were of the highest quality and purchased from "Sigma-Aldrich Co. (St. Louis, MO, USA)". Solvents were used as received without more purifications.

2.2. Pipemidic Acid Complexes' Synthesis

A methanolic fluid of 1 mmol metal salt chlorides ($MgCl_2.6H_2O$, $CaCl_2.2H_2O$, $ZnCl_2$ and $FeCl_3.6H_2O$) and 1 mmol of pipemidic acid drug (pipH) were dissolved to form homogeneous mixtures. The complex solutions were neutralized at pH ~ 7–8 using a few drops of NH_3 solution; then, the mixtures were refluxed with contentiously stirring for three hours. All colored combinations were then cooled to ambient conditions until they aggregated and could be filtered, washed several times with hot CH_3OH to get rid of the unreacted portions, and left to dry at 75 °C. Using TLC plates, the purity of pip complexes was examined. There have been several unsuccessful trials to produce one pure crystal appropriate for "X-ray crystallography". These solid complexes are isolated with the anhydrous statement and high melting points due to thermal stabilities. Nevertheless, the spectral and thermogravimetric outcomes could be appropriate to propose the envisaged structures of arrangement for synthesized "$[Mg(pip)(H_2O)_3(Cl)].6H_2O$, $[Ca(pip)(H_2O)_3(Cl)].2H_2O$, $[Zn(pip)(H_2O)_3(Cl)].4H_2O$, and $[Fe(pip)(H_2O)_2(Cl)_2].6H_2O$", (where pip = deprotonated pipemidic) drug complexes (Figure 2).

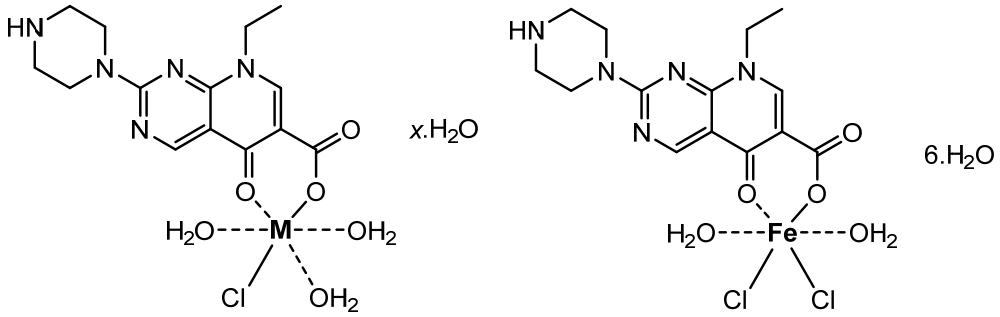


Figure 2. Suggested structures of pipemidic acid (pip)–magnesium, calcium, zinc, and iron (III) drug complexes (M = Mg^{II} (x = 6), Ca^{II} (x = 2), and Zn^{II} (x = 4)).

2.3. Instrumentals

1. The elemental analyses of carbon, hydrogen and nitrogen contents were performed by the microanalysis unit at Cairo University, Egypt, using a Perkin Elmer CHN 2400 (USA).

2. The molar conductivities of freshly prepared 1.0×10^{-3} mol/cm^3 dimethyl sulfoxide (DMSO) solutions were measured for the soluble pipemidic acid complexes using the Jenway 4010 conductivity meter.

3. The infrared spectra with KBr discs were recorded on a Bruker FT-IR Spectrophotometer (4000–400 cm^{-1}) with a resolution of 4 cm^{-1} with 50 successive scans.

4. UV–Vis. absorption spectra by UV2 Unicam UV/Vis Spectrophotometer, DMSO solvent, 800–200 nm range, quartz cell of 1.0 cm path length.

5. Magnetic susceptibility measurements of pipemidic acid complexes were taken at room temperature (25 °C) using a Sherwood Scientific Magway MSB MK1 model magnetic balance by the Gouy method using $Hg[Co(SCN)_4]$ as the calibrant.

6. The thermal studies TG/DTG–50H were carried out on a Shimadzu thermogravimetric analyzer under N_2 gas till 800 °C; the rate of heating was kept at 10 °C/min.

7. X-ray powder diffraction patterns for pipemidic acid and its complexes were collected on a Philips X'pert Pro diffractometer in transmission mode with focusing mirror and 1-D PSD detector. The compounds were finely grounded in the mortar and loaded into capillaries (1 mm diameter). The patterns were collected at 25 °C using CuKα radiation (counting time: 9 s/step; 2θ ranges: 4–90°).

8. Transmission electron microscopy (TEM) and high-resolution transmission electron microscopy (HRTEM) images were recorded with a Jeol JEM-100s scanning transmission electron microscope. The morphology of the samples was examined in transmission electron microscopy operating at voltage of 80 kV.

3. Results and Discussion

3.1. Microanalytical and Conductance Measurements

The microanalytical and physical results of the pipemidic acid (pip) coordinated complexes are mentioned as follows: both theoretical and experimental elementary data are well agreed (Table 1).

These findings showed that the ligand had a 1:1 molar ratio of coordination to the complex cations of magnesium, calcium, zinc, and iron. In the air, any construct that has been created is stable. Solid pip complexes are insoluble in water, EtOH, CHCl3, acetone, and cyclohexane. The complexes are substantially more stable than the ligand, as evidenced by the freezing temperatures of the complexes being greater than those of the pipH ligand. The complexes' molar conductance values (estimated in 10^{-3} M DMSO solvent at ambient conditions) lay in the range of 18–28 $\Omega^{-1}cm^2mol^{-1}$ at 25 °C, which indicates that all complexes have a non-electrolytic nature [22]. Based on the deprotonation of the carboxylic group or maybe anion exhibits inside the chelating sphere, these result data are attributed to the lack of chloride ions. So, by comparing the degree of ionization of the complexes with experimental values of electrolyte materials, it was possible to verify the presence of

Cl (ions inside the coordination sphere) [22]. According to this result date, the chlorine atoms are located inside the coordination sphere, which was tested using $AgNO_3$ reagent. The percentage of metal ions (magnesium, calcium, zinc, and iron) was calculated using the gravimetry approach in the form of stable metal oxides.

Table 1. Microanalytical and physical data of pipemidic acid complexes.

Complexes/ F·Wt	Color	Yield	M.Wt/g/mol	Mp/°C	$\Lambda_{M/}$ $\Omega^{-1}\cdot cm^2\cdot mol^{-1}$	Elemental Analysis Found (Calcd.)			
						%C	%H	%N	%M
Complex 1 $MgC_{14}H_{34}N_5O_{12}Cl$	pale yellow	77%	524	>300	18	31.98 (32.08)	6.42 (6.54)	13.34 (13.36)	4.61 (4.64)
Complex 2 $CaC_{14}H_{26}N_5O_8Cl$	yellow	74	468	>300	21	35.77 (35.94)	5.51 (5.60)	14.92 (14.97)	8.46 (8.57)
Complex 3 $ZnC_{14}H_{30}N_5O_{10}Cl$	yellow	77	529	>300	24	31.31 (31.77)	5.59 (5.71)	12.95 (13.23)	12.18 (12.35)
Complex 4 $FeC_{14}H_{32}N_5O_{11}Cl_2$	brown	72	573	>300	28	29.30 (29.34)	5.60 (5.63)	12.10 (12.22)	9.71 (9.74)

$[Mg(pip)(H_2O)_3(Cl)].6H_2O$ complex 1; $[Ca(pip)(H_2O)_3(Cl)].2H_2O$ complex 2; $[Zn(pip)(H_2O)_3(Cl)].4H_2O$ complex 3; $[Fe(pip)(H_2O)_2(Cl)_2].6H_2O$ complex 4.

3.2. Infrared Assignments

The infrared spectral regions were identified by the comparison of complexes' spectra to those of the free pipH ligand (Figure 3 and Table 2). The infrared spectra of the new complexes, "$[Mg(pip)(H_2O)_3(Cl)].6H_2O$, $[Ca(pip)(H_2O)_3(Cl)].2H_2O$, $[Zn(pip)\ (H_2O)_3(Cl)].4H_2O$, and $[Fe(pip)(H_2O)_2(Cl)_2].6H_2O$", (Figure 2) within the most important region in the infrared spectra of these four complexes and the pipemidic acid-free ligand (~1800–1200 cm^{-1}) are selected and assigned in Table 1 and displayed in Figure 3A–E. The assignments data of (pip)–magnesium, calcium, zinc, and iron (III) drug complexes show no absorption band at ~1770 cm^{-1}, which is characteristic of the stretching vibration ν(C=O) of the carboxylic group, which is suggestive of the contribution of the carboxyl group in the matching with the metal ion. The peak at 1618-to-1607 cm^{-1} is present in the spectral data of the pipemidic acid complexes and can be allocated to the asymmetric stretching vibration of the carboxylate group, $\nu_{as}(COO^-)$. The spectra of Mg(II), Ca(II), Zn(II), and Fe(III) complexes also have a medium-to-strong intensity band within the 1421-to-1351 cm^{-1} region. Because of its significance in interpreting the symmetric vibration of the vs. (COO^-) group, this band is absent from the spectra of pipH. The criteria that can be utilized to discriminate between the three binding states of the carboxylate complexes have been investigated by Deacon and Phillips [23–29]. These prerequisites are (i) $\Delta\nu > 200\ cm^{-1}$ (where $\Delta\nu = [\nu_{as}(COO^-) - \nu_s(COO^-)]$) for which the same connection is observed in the case of unidentified carboxylato complexes; (ii) bidentate or chelating carboxylato complexes exhibit Δν appreciably less than ionic values($\Delta\nu < 100\ cm^{-1}$); and finally, (iii) bridging complexes reveal Δν equivalent to ionic values ($\Delta\nu \sim 150\ cm^{-1}$). The noticed Δν for the (pip)–magnesium, calcium, zinc, and iron (III) drug complexes are 217, 263, 256, and 252 cm^{-1}, respectively, which endorse unidentate chelation of the COO^-. The infrared spectral information of the pipH free ligand reveals a band at 1628 cm^{-1} due to the widening vibration of R_2CO of pyridopyrimidine moiety. This band was shifted to a lower wavenumber (1557-to-1537 cm^{-1}), which indicated that the oxygen of the carbonyl group is involved in the coordination of the metal ions [30]. The assignments of the widening vibrations of ν(M–O) in structures are observed within the "500–600 cm^{-1}" range [30]. The interplay of elements of Mg(II), Ca(II), Zn(II), and Fe(III) complexes are well-known in an octahedral geometry.

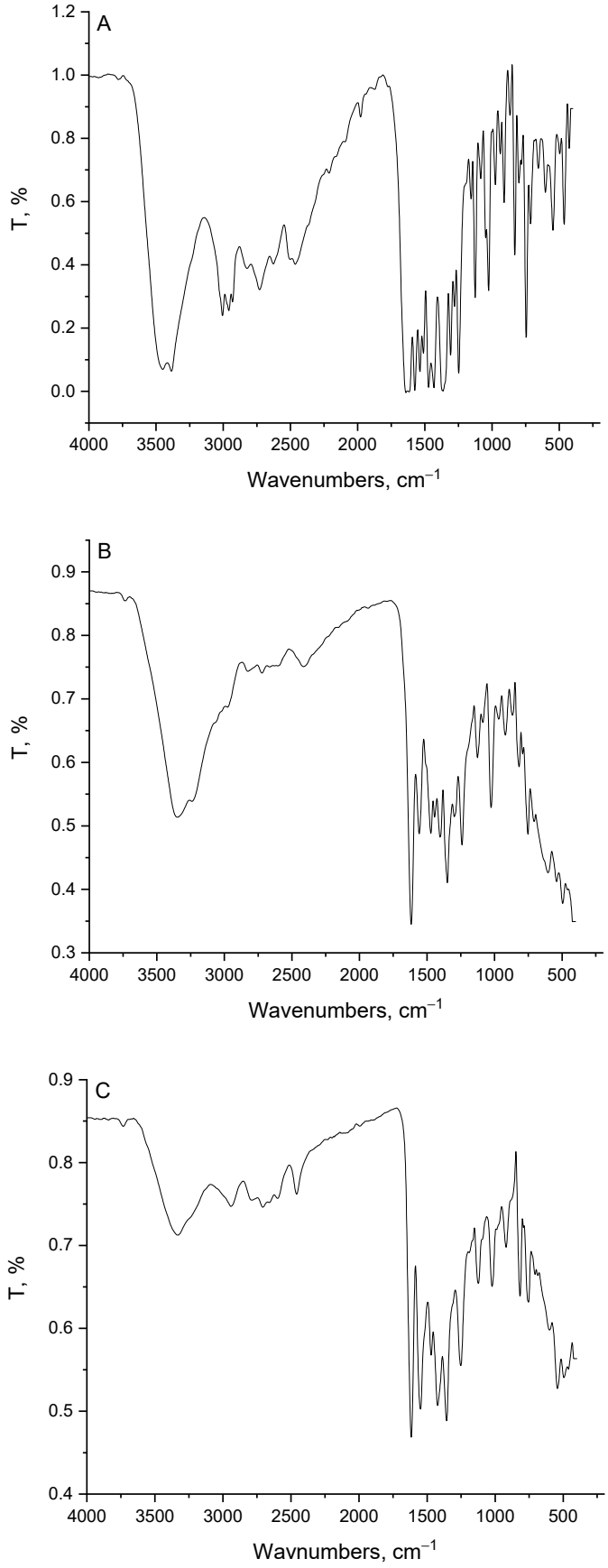


Figure 3. *Cont.*

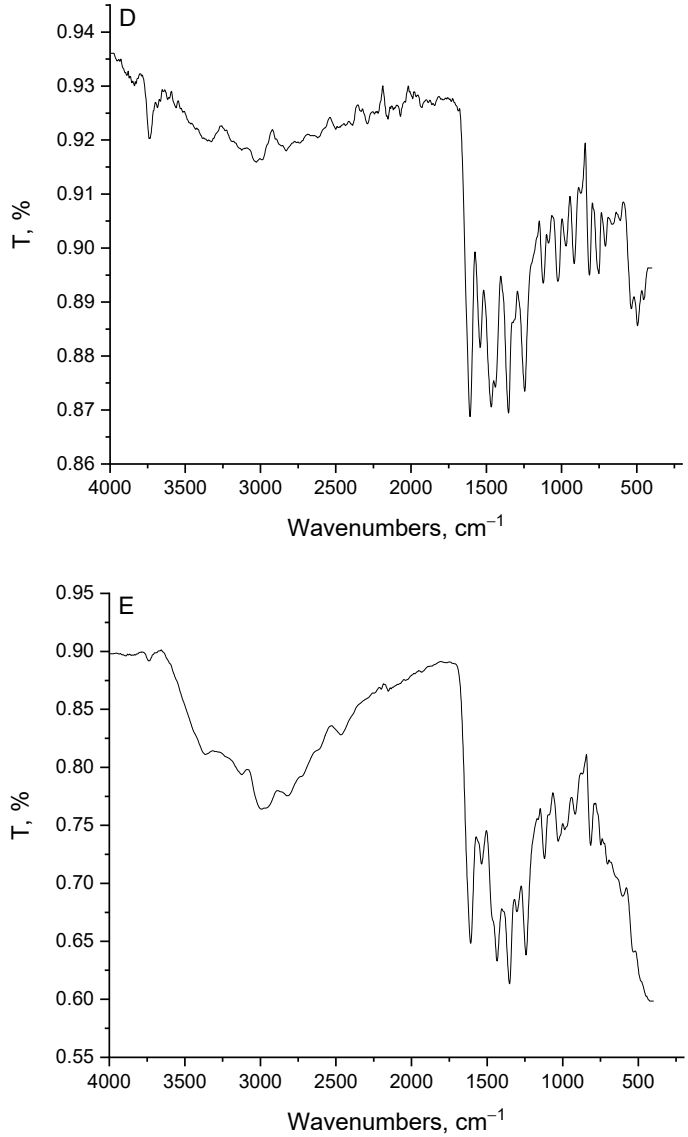


Figure 3. Infrared spectra of (**A**): pipH free ligand and its complexes (**B**): Mg(II), (**C**): Ca(II), (**D**): Zn(II), and (**E**): Fe(III).

3.3. Electronic Spectral Data of [Fe(pip)(H$_2$O)$_2$(Cl)$_2$].6H$_2$O Complex

Iron's spectral data of [Fe(pip)(H$_2$O)$_2$(Cl)$_2$].6H$_2$O complex display bands at 455 and 348 cm^{-1} assigned to $^6A_1g \rightarrow {}^4T_2g$ (G) and $^6A_1g \rightarrow {}^4Eg$ (G) transitions, respectively, in an octahedral geometry [31]. The magnetic moment value is at 4.80 BM, which agrees with iron's high spin octahedral configuration (III). The Mg(II), Ca(II), and Zn(II) complexes are diamagnetic and were found to have an octahedral geometry.

Powder X-ray Diffraction and TEM Morphology

The X-ray powder diffractions of [Mg(pip)(H$_2$O)$_3$(Cl)].6H$_2$O, [Ca(pip)(H$_2$O)$_3$(Cl)].2H$_2$O, [Zn(pip)(H$_2$O)$_3$(Cl)].4H$_2$O, and [Fe(pip)(H$_2$O)$_2$(Cl)$_2$].6H$_2$O (where, pip = deprotonated pipemidic) solid complexes **1–4** are shown in Figure 4. Crystalline to amorphous states are seen in these diffraction patterns. Using the Debye–Scherrer formula (Equation (1)), the particle size (D) of pip complexes **1–4** was estimated from the principal diffraction patterns of each obtained compound [32,33].

$$D = \frac{K\lambda}{\beta \cos\theta} \quad (1)$$

Table 2. FTIR frequencies (cm^{-1}) and assignments of pipH free ligand, pip–magnesium, calcium, zinc, and iron (III) drug complexes.

pipH	Mg(II)	Ca(II)	Zn(II)	Fe(III)	Assignments *
3454, 3383	3348	3333	3327	3363	ν(N-H) + ν_{as}(O-H); H_2O
3005, 2955 2929, 2818 2728, 2621	3237, 2969 2823	2939, 2788	3131, 3020 2823	3125, 2984 2818	ν_s(O-H) + ν(C-H)
1774	–	–	–	–	ν(C=O): (COOH)
–	1618	1618	1607	1607	$\nu_{as}(COO^-)$
1628, 1573	1557	1548	1543	1537	ν(C=O) + $\delta_b(H_2O)$ Phenyl breathing modes
1537, 1507 1471, 1432	1471, 1441	1466, 1421	1467	1432	CH; deformation of $–CH_2–$
–	1401	1355	1351	1355	$\nu_s(COO^-)$
1366	1346	1310	1330	1300	$\delta_b(CH_2)$
1280, 1250	1295, 1244	1250	1244	1239	ν(C-C)
1159	1128	1124	1124	1119	ν(C-O) + ν(C-N)
1128, 1083 1023, 972	1023	1017	1023	1028	$\delta_r(CH_2)$
942, 906 867, 826 801	922, 861	917, 816	912, 817	912, 816	CH- bend; phenyl
745	784	756	751, 705	751	$\delta_b(COO^-)$
654, 604 543, 423	604, 543 493	599, 543 493, 458	660, 610 539, 493, 453	599, 534	ν(M-O) + ring deformation

* ν, stretching & δ, bending.

Cu K radiation has an X-ray wavelength (λ) of 1.5418 Å; *K* is constant and is considered to be 0.94, the full width at half maximum (FWHM) of a significant intensity peak (a peak with 100% relative intensity), and the peak position. According to the Deby–Scherrer formula, the grain sizes for the Mg(II), Ca(II), Zn(II), and Fe(III) complexes were 2, 18, 17, and 37 nm, respectively.

Table 2 contains a list of the gathered XRD data, including 2θ, strengths, and d-spacing. The production of high-quality complexes is indicated by the dislocation density (δ), which was calculated from Equation (2) [34] and presented in Table 3.

$$\delta = \frac{1}{D^2} \quad (2)$$

Table 3. Data on crystallite diameters (D), dislocation density (δ), 2, intensities, and d-spacing of pip complexes **1**–**4** were acquired using XRD.

Complexes	D (nm)	δ ($10^{12}\cdot lin\cdot m^{-2}$)	2Theta	Intensity	d-Value (nm)
Complex **1**	2	0.2500	16	100	0.55
Complex **2**	18	0.0031	26	100	0.34
Complex **3**	17	0.0035	12	100	0.74
Complex **4**	37	0.0007	12	100	0.74

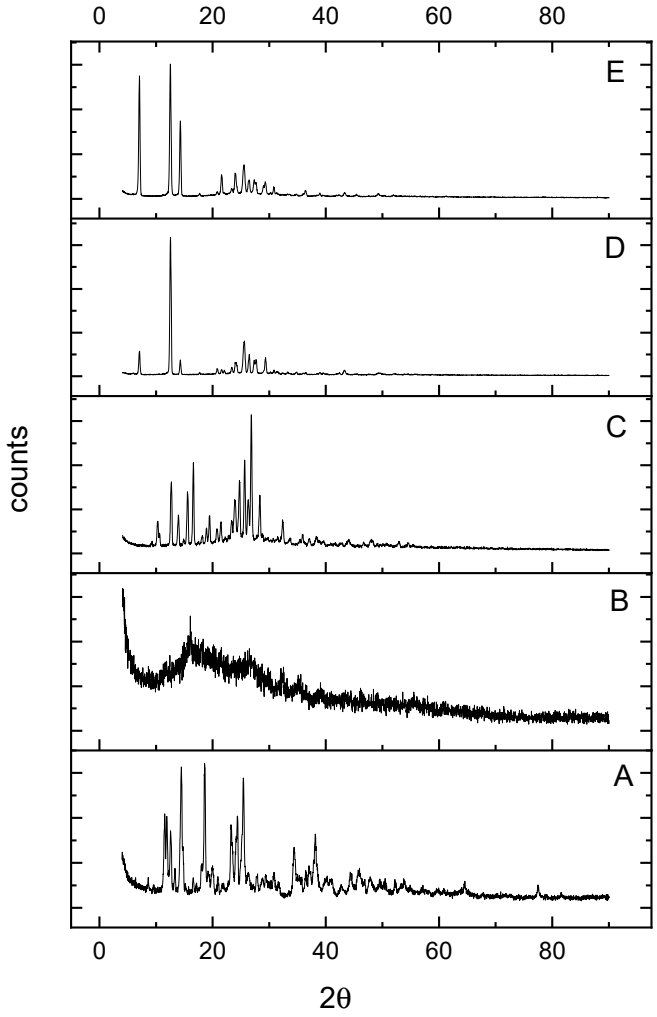


Figure 4. X-ray powder diffraction patterns of (**A**): pipH, (**B**): Mg(II), (**C**): Ca(II), (**D**): Zn(II), and (**E**): Fe(III)–pip complexes.

TEM photos of pip complexes **1–4** (Figure 5A–D) confirm the presence of spherical NPs, which appeared as black spots.

3.4. Thermal Studies

The $[Mg(pip)(H_2O)_3(Cl)].6H_2O$, $[Ca(pip)(H_2O)_3(Cl)].2H_2O$, $[Zn(pip)(H_2O)_3(Cl)].4H_2O$, and $[Fe(pip)(H_2O)_2(Cl)_2].6H_2O$, (where, pip = deprotonated pipemidic) solid complexes **1–4** are stable at room temperature. These complexes were discussed using thermogravimetric (TGA) examination from room conditions to 500 °C under N_2 gas. The Resketched TGA Plot showed the percent mass loss against temperature (°C) (Figure 6). In Table 4, along with evolved moiety and theoretical percentage mass losses, the temperature variations and mass percentage losses of the breakdown processes are listed. The overall mass loss from the TGA curves is 92.96% for Mg(II) complex, 78.67%% for Ca(II) complex, 84.55%% for Zn(II) complex, and 87.55% for the iron(III) complex, respectively. All complexes exhibit a two- to three-stage mass decrease in their TGA curves. The creation of their respective anhydrous chemicals corresponds to the initial mass loss. The disintegration of coordinated ligands, such as coordinated water molecules and chlorine atoms next to the pip ($C_{14}H_{16}N_5O_3$) particles, is what causes the second and third mass losses. The leftover items were verified using infrared bands.

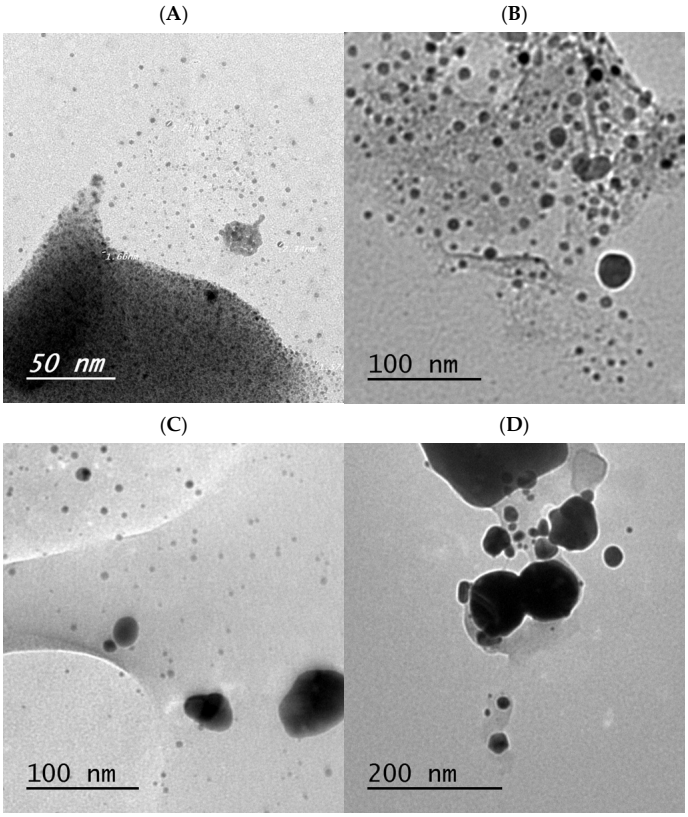


Figure 5. TEM images of (**A**): Mg(II), (**B**): Ca(II), (**C**): Zn(II), and (**D**): Fe(III)–pip complexes.

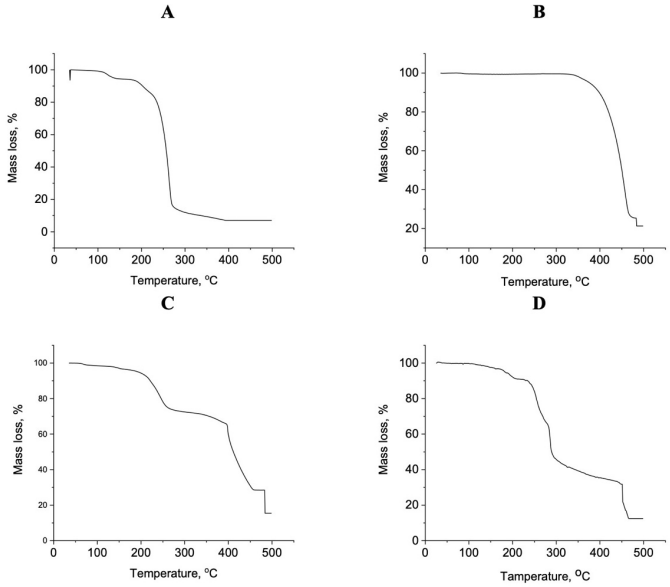


Figure 6. TGA curves of (**A**): Mg(II), (**B**): Ca(II), (**C**): Zn(II), and (**D**): Fe(III)–pip complexes.

3.5. Kinetics Data

Two often referenced techniques for calculating the kinetic thermodynamic parameters in the literature are Coats–Redfern [35] and Horowitz–Metzger [36]. In this study, these two approaches are used. The following equations were used in conjunction with well-known techniques to compute the activation energy, E; pre-exponential factor, A; entropies, ΔS; enthalpy ΔH; and Gibbs free energy, ΔG, from the TGA curves.

$$\Delta H = E - RT \text{ and } \Delta G = \Delta H - T\,\Delta S$$

Table 4. TGA data for the Mg(II), Ca(II), Zn(II), and Fe(III)–pip complexes.

Samples	Stage	TGA Range (°C)	DTG Peak (°C)	Weight Loss (%)		Evolved Moiety
				Found	Calc	
Mg(II) complex	I	30–180	150	20.55	20.61	$6H_2O$
	II	180–270	250	17.10	17.08	$3H_2O + \frac{1}{2}Cl_2$
	III	270–500	330	55.31	54.58	$C_{14}H_{16}N_5O_2$
	Residue			7.04	7.73	MgO
Ca(II) complex	I	30–300	260	26.91	26.82	$5H_2O + \frac{1}{2}Cl_2$
	II	300–500	430	51.76	51.71	$C_{13}H_{16}N_5$
	Residue			21.33	21.47	$CaCO_3$
Zn(II) complex	I	30–250	200	13.65	13.61	$4H_2O$
	II	250–400	320	17.10	16.92	$3H_2O + \frac{1}{2}Cl_2$
	III	400–500	420	53.80	54.06	$C_{14}H_{16}N_5O_2$
	Residue			15.45	15.41	ZnO
Fe(III) complex	I	30–230	150	18.90	18.85	$6H_2O$
	II	230–300	270	18.82	18.67	$2H_2O + Cl_2$
	III	300–500	330, 450	49.83	49.91	$C_{14}H_{16}N_5O_2$
	Residue			12.45	12.57	FeO

Table 5 includes a summary of the kinetic parameters for the second breakdown stage as well as the ionic radius of metal ions. These values were estimated using the Coats–Redfern and Horowitz–Metzger equations. The findings demonstrate that the values produced using different techniques are equivalent. The kinetic data collected using the two approaches agree with one another. Mg(II), Ca(II), Zn(II), and Fe(III) compound activation energies are anticipated to rise in correlation with a reduction in their radius [37–40]. The ligand may go closer since the ionic radius is less. As a result, the Fe(III) complex's E value in the second stage is larger than that of the other complexes [37,40].

Table 5. Kinetic thermodynamic parameters data of the pip complexes.

Complexes	Ionic Radius/pm	Parameters *	Coats-Redfern eq.	Horowitz-Metzger eq.
Mg(II) complex	0.72Å	E	2.44E+05	2.54E+05
		A	2.27E+22	5.22E+23
		ΔS	1.78E+02	2.04E+02
		ΔH	2.40E+05	2.50E+05
		ΔG	1.46E+05	1.42E+05
Ca(II) complex	0.99Å	E	1.54E+05	1.74E+05
		A	1.54E+09	6.71E+10
		ΔS	−7.62E+01	−4.49E+01
		ΔH	1.48E+05	1.68E+05
		ΔG	2.02E+05	2.00E+05
Zn(II) complex	0.74 Å	E	1.93E+05	2.03E+05
		A	2.92E+12	2.58E+13
		ΔS	−1.33E+01	4.83E+00
		ΔH	1.87E+05	1.97E+05
		ΔG	1.96E+05	1.94E+05
Fe(III) complex	0.645 Å	E	3.10E+05	3.83E+05
		A	5.87E+05	6.98E+00
		ΔS	−1.40E+02	−2.35E+02
		ΔH	2.61E+04	3.33E+04
		ΔG	1.10E+05	1.74E+05

* Units of parameters: E/kJmole^{-1}, A/s^{-1}, ΔS/Jmole^{-1}k^{-1}, ΔH and ΔG/kJmole^{-1}.

4. Conclusions

Four new solid complexes of pipemidic acid (pipH) with Mg^{2+}, Ca^{2+}, Zn^{2+}, and Fe^{3+} were synthesized and characterized. Pipemidic acid acts as bidentate chelate through the oxygen atoms of both carboxylate and carbonyl groups of pyridopyrimidine ring. The spectroscopic data revealed that general formulas of pipH complexes are $[Mg(pip)(H_2O)_3(Cl)].6H_2O$, $[Ca(pip)(H_2O)_3(Cl)].2H_2O$, $[Zn(pip)(H_2O)_3(Cl)].4H_2O$, and $[Fe(pip)(H_2O)_2(Cl)_2].6H_2O$. The number of water molecules with their locations inside or outside the coordination sphere were assigned via thermal analyses (TG, DTG). DTG curves refer to 2–3 thermal decomposition steps where the first decomposition step at lower temperature corresponds to the loss of uncoordinated water molecules followed by decomposition of pip molecule at higher temperatures. Thermodynamic parameters (E*, ΔS*, ΔH*, and ΔG*) were calculated from TG curves using Coats–Redfern and Horowitz–Metzger non–isothermal models. X-ray powder diffraction (XRD) and transmission electron microscopy (TEM) techniques were carefully used to assign properly the particle size of the prepared pip complexes.

Funding: The Deanship of Scientific Research at Princess Nourah bint Abdulrahman University, Riyadh, Saudi Arabia through Researchers Supporting Project number (PNURSP2023R35).

Data Availability Statement: Data recorded in the current study is available in all Tables and Figures of the manuscript.

Acknowledgments: The author is grateful to Princess Nourah bint Abdulrahman University, Riyadh, Saudi Arabia for funding this work through Researchers Supporting Project number (PNURSP2023R35).

Conflicts of Interest: The authors declare no conflict of interest.

References

1. EMA. Disabling and potentially permanent side effects lead to suspension or restrictions of quinolone and fluoroquinolone antibiotics. *Eur. Med. Agency* **2018**, *31*, 1–3.
2. Zaki, A.; Schreiber, E.C.; Weliky, I.; Knill, J.R.; Hubsher, H.J. Clinical pharmacology of oral cephradine. *J. Clin. Pharmacol.* **1974**, *14*, 1180. [CrossRef] [PubMed]
3. Anacona, J.R. Synthesis and antibacterial activity of some metal complexes of beta-lactamic antibiotics. *J. Coord. Chem.* **2001**, *54*, 355. [CrossRef]
4. Lozano, J.; Borras, J. Antibiotic as ligand. Coordinating behavior of the cephalexin towards Zn (II) and Cd (II) ions. *J. Inorg. BioChem.* **1987**, *31*, 187. [CrossRef]
5. Abdel-Gawad, F.M.; El-Guindi, N.M.; Ibrahim, M.N. Cephalexin complexes with some 3d transition-metal ions. *J. Drug Res.* **1987**, *17*, 197.
6. Helaleh, M.I.H.; Nameh, E.S.M. Selective kinetic study for the degradation of cephalexin in alkaline aqueous media. *An. Quim. Int. Ed.* **1998**, *94*, 160.
7. Sorenson, J.R.J. Copper chelates as possible active forms of the antiarthritic agents. *J. Med. Chem.* **1976**, *19*, 135. [CrossRef]
8. Brown, D.H.; Lewis, A.E.; Smith, W.E.; Teape, J.W. Antiinflammatory effects of some copper complexes. *J. Med. Chem.* **1980**, *23*, 729. [CrossRef] [PubMed]
9. Williams, D.R. *The Metals of Life*; Van Nostrand Reinhold: London, UK, 1971.
10. Ruiz, M.; Perello, L.; Ortiz, R.; Castineiras, A.; Maichlemossmer, C.; Canton, E. Synthesis, characterization, and crystal structure of [Cu (cinoxacinate) 2]· 2H2O complex: A square-planar CuO4 chromophore. Antibacterial studies. *J. Inorg. Biochem.* **1995**, *59*, 801. [CrossRef] [PubMed]
11. Castillo-Blum, S.E.; Barba-Behrens, N. Coordination chemistry of some biologically active ligands. *Coord. Chem. Rev.* **2000**, *196*, 3. [CrossRef]
12. Naglah, A.M.; Al-Omar, M.A.; Almehizia, A.A.; AlKahtani, H.M.; Bhat, M.A.; Al-Shakliah, N.S.; Belgacem, K.; Majrashi, B.M.; Refat, M.; Adam, A.M.A. Synthesis, thermogravimetric, and spectroscopic characterizations of three palladium metal(II) ofloxacin drug and amino acids mixed ligand complexes as advanced antimicrobial materials. *J. Mol. Struct.* **2021**, *1225*, 129102. [CrossRef]
13. Refat, M.S.; Saad, H.A.; Gobouri, A.A.; Alsawat, M.; Adam, A.M.A.; Shakya, S.; Gaber, A.; Alsuhaibani, A.M.; El-Megharbel, S.M. Synthesis and spectroscopic characterizations of nanostructured charge transfer complexes associated between moxifloxacin drug donor and metal chloride acceptors as a catalytic agent in a recycling of wastewater. *J. Mol. Liq.* **2021**, *349*, 118121. [CrossRef]
14. Alibrahim, K.A.; Al-Saif, F.A.; Alghamdi, M.; El-Shahawi, M.; Althubeiti, K.; Aljuhani, E.; Refat, M. Spectroscopic, molecular structural, thermal, biological and voltammetric characterization of Ru3+, Pt4+and Ir3+complexes of lomefloxacin drug. *Lat. Am. J. Pharm.* **2019**, *38*, 1077–1090.

15. Naglah, A.M.; Al-Omar, M.A.; Almehizia, A.A.; Obaidullah, A.J.; Bhat, M.A.; Al-Shakliah, N.S.; Belgacem, K.; Majrashi, B.M.; Refat, M.; Adam, A.M.A. Synthesis, spectroscopic, and antimicrobial study of binary and ternary ruthenium(III) complexes of ofloxacin drug and amino acids as secondary ligands. *Crystals* **2020**, *10*, 225. [CrossRef]
16. Refat, M.; El-Sayed, M.Y.; Hassan, R.F. Study of the chemical structure and the microbial effect of the iron(III) metal ions with four consecutive generations of quinolones in a nanometric form for the purpose of raising the efficacy of anti-bacterial and fungal drugs. *Appl. Organomet. Chem.* **2018**, *32*, e4195. [CrossRef]
17. Al-Saif, F.A.; Alibrahim, K.A.; Alfurhood, J.A.; Refat, M. Synthesis, spectroscopic, thermal, biological, morphological and molecular docking studies of the different quinolone drugs and their cobalt(II) complexes. *J. Mol. Liq.* **2018**, *249*, 438–453. [CrossRef]
18. El-Megharbel, S.M.; Hegab, M.S.; Manaaa, E.-S.A.; Al-Humaidi, J.Y.; Refat, M.S. Synthesis and physicochemical characterizations of coordination between palladium(II) metal ions with floroquinolone drugs as medicinal model against anticancer cells: Novel metallopharmaceuticals. *New J. Chem.* **2018**, *42*, 9709–9719. [CrossRef]
19. Alibrahim, K.A.; Al-Saif, F.A.; Alghamdi, M.; El-Shahawi, M.S.; Moustafa, Y.M.; Refat, M.S. Synthesis, spectroscopic, thermal, antimicrobial and electrochemical characterization of some novel Ru(III), Pt(IV) and Ir(III) complexes of pipemidic acid. *RSC Adv.* **2018**, *8*, 22515–22529. [CrossRef]
20. Alghamdi, M.T.; Alsibaai, A.A.; Shahawi, M.S.; Refat, M.S. Structural and chelation behaviors of new Ru(III), Pt(IV) and Ir(III) gatifloxacin drug complexes: Spectroscopic characterizations. *J. Mol. Struct.* **2017**, *1130*, 264–275. [CrossRef]
21. Hussien, M.A.; El-Megharbel, S.M.; Refat, M.S. In-situ copper(II) complexes of some quinolone drug ligands were discussed for their molecular structures: Synthesis in binary solvent. *J. Comput. Theor. Nanosci.* **2017**, *14*, 561–576.
22. Geary, W.J. The use of conductivity measurements in organic solvents for the characterisation of coordination compounds. *Coord. Chem. Rev.* **1971**, *7*, 81. [CrossRef]
23. Chen, Z.-F.; Li, B.-Q.; Xie, Y.-R.; Xiong, R.-G.; You, X.-Z.; Feng, X.-L. Synthesis, crystal structure, and characterization of mixed-ligand complex of copper (I) with drug of norfloxacin and triphenyl phosphine:[Cu (PPh3) 2 (H-Norf)] ClO4. *Inorg. Chem. Commun.* **2001**, *4*, 346. [CrossRef]
24. Wang, L.-Z.; Chen, Z.-F.; Wang, X.-S.; Li, Y.-H.; Xiong, R.-G.; You, X.-Z. 2D nanoporous molecular square grid: Manganese (II) norfloxacin complex. *Chin. J. Inorg. Chem.* **2002**, *18*, 1185.
25. Chen, Z.-F.; Liang, H.; Hu, H.-M.; Li, Y.; Xiong, R.-G.; You, X.-Z. A neutral 2D nanosized molecular square grid: The first vanadium(II)coordination polymer of norfloxacin. *Inorg. Chem. Commun.* **2003**, *6*, 241. [CrossRef]
26. Li, Y.-X.; Chen, Z.-F.; Xiong, R.-G.; Xue, Z.; Ju, H.-X.; You, X.-Z. A mononuclear complex of norfloxacin with silver (I) and its properties. Inorg. *Chem. Commun.* **2003**, *6*, 819.
27. Nakamoto, K. *Infrared and Raman Spectra of Inorganic and Coordination Compounds*; Wiely: New York, NY, USA, 1978.
28. Ross, S.D. *Inorganic Infrared and Raman Spectra*; McGraw Hill: London, UK, 1972.
29. Deacon, G.B.; Phillips, R.J. Relationships between the carbon-oxygen stretching frequencies of carboxylato complexes and the type of carboxylate coordination. *Coord. Chem. Rev.* **1980**, *33*, 227. [CrossRef]
30. Silverstein, R.M.; Bassler, G.C.; Morril, T.C. *Spectroscopic Identification of Organic Compounds*, 5th ed.; Wiley: New York, NY, USA, 1991.
31. Anuradha, S.; Pramila, S. Synthesis, characterization, in-vitro anti-inflammatory and antimicrobial screening of metal (II) mixed diclofenac and acetaminophen complexes. *Indian J. Chem.* **2000**, *39*, 874–876.
32. Cullity, B.D. *Elements of X-ray Diffraction*; Addison-Wesley, Reading: Boston, MA, USA, 1972; p. 102.
33. Salavati-Niasari, M.; Mohandes, F.; Davar, F.; Mazaheri, M.; Monemzadeh, M.; Yavarinia, N. Preparation of NiO nanoparticles from metal-organic frameworks via a solid-state decomposition route. *Inorg. Chim. Acta* **2009**, *362*, 3691. [CrossRef]
34. Velumani, S.; Mathew, X.; Sebastian, P.J. Structural and optical characterization of hot wall deposited CdSexTe1− x films. *Solar Energy Mater. Solar Cells* **2003**, *76*, 359. [CrossRef]
35. Coats, A.W.; Redfern, J.P. Kinetic parameters from thermogravimetric data. *Nature* **1964**, *201*, 68. [CrossRef]
36. Horowitz, H.H.; Metzger, G. A new analysis of thermogravimetric traces. *Anal. Chem.* **1963**, *35*, 1464. [CrossRef]
37. Wendlandt, W.W. *Thermal Methods of Analysis*; Interscience: New York, NY, USA, 1964.
38. Avsar, G.; Kulcu, N.; Arslan, H. Thermal behaviour of copper (II), nickel (II), cobalt (II) and palladium (II) complexes of N, N-dimethyl-N′-benzoylthiourea. *Tur. J. Chem.* **2002**, *26*, 607.
39. Sodhi, G.S. Correlation of thermal stability with structures for some metal complexes. *Therm. Chim. Acta* **1987**, *120*, 107. [CrossRef]
40. Arslan, H.; Ozpozan, N.; Tarkan, N. Kinetic analysis of thermogravimetric data of *p*-toluidino-*p*-chlorophenylglyoxime and of some complexes. *Therm. Chim. Acta* **2002**, *383*, 69. [CrossRef]

Disclaimer/Publisher's Note: The statements, opinions and data contained in all publications are solely those of the individual author(s) and contributor(s) and not of MDPI and/or the editor(s). MDPI and/or the editor(s) disclaim responsibility for any injury to people or property resulting from any ideas, methods, instructions or products referred to in the content.